ChemComm

COMMUNICATION

View Article Online
View Journal | View Issue

Cite this: *Chem. Commun.*, 2025, **61**, 4820

Received 6th October 2024,
Accepted 14th February 2025

DOI: 10.1039/d4cc05248j

rsc.li/chemcomm

Small organic fluorophores with SWIR emission detectable beyond 1300 nm†

Michal Pieczykolan,[a] Pierre Alix Dancer,[b] Tjadina-Wencke Klein,[cdefg] Hubert Piwonski,[h] Hannes Rolbieski,[g] Bholanath Maity,[i] Oliver T. Bruns,[cdefg] Luigi Cavallo,[i] Fabian Kiessling,[j] Magnus Rueping[ij] and Srinivas Banala[*aij]

3,6-Dimethylamino fluorenone was functionalized with substituents to achieve an absorption maximum at 1012 nm and emission >1300 nm. TD-DFT calculations confirmed that the substituent orbitals contribute to narrowing the HOMO–LUMO energy gap. Imaging with an InGaAs-based SWIR camera and various longpass filters confirmed detection >1300 nm.

Fluorescence-based imaging techniques (fluorescence reflectance imaging FRI, and fluorescence molecular tomography FMT) have revolutionized non-invasive bioimaging of living subjects,[1] including the movement of biomolecules, the fate of drug molecules,[2] and the detection of metabolites as well as short-lived species. FRI and FMT imaging have primarily been used in the wavelengths of near infrared (NIR, *i.e.*, absorption and emission, $\lambda_{abs}/\lambda_{Em}$, 650–900 nm). This has been motivated by improved penetration depth of NIR light compared to the visible part of the spectrum.[3] However, contrast and resolution in tissue improves significantly with increasing wavelengths beyond 1000 nm. Furthermore, longer wavelengths are advantageous due to their reduced phototoxicity, lower photon scattering and inherently low tissue autofluorescence, thus demonstrating huge potential for safe and effective *in vivo* imaging. Consequently, imaging techniques utilizing wavelengths in the shortwave infrared (SWIR, 1000–2000 nm) are being explored to enhance deep tissue imaging capabilities for clinical applications.[4–6] The properties of the applied fluorophores are critical in determining the imaging outcomes, prompting the development of various materials for use in SWIR imaging.[7] To date, studies have investigated inorganic[8,9] and organic nanomaterials,[10] semiconducting polymers[11] and recently also small-molecule organic dyes.[12–15]

Among the organic dyes, indocyanine green (ICG) is an FDA approved chromophore with $\lambda_{abs}/\lambda_{Em}$ in the NIR-range. Due to its tail emission in the SWIR window, ICG has gained significant attention for SWIR imaging.[16] ICG analogues, such as IRDye800CW and IR-12N3, have also been extensively studied.[17–19] Inspired by these results, other cyanines have been engineered to obtain SWIR emissions. For instance, indolenines in polymethine have been modified with electron-rich donors, such as dimethyl-flavylium (Flav 7),[20] or rigid thiopyrylium heterocycles (5H5).[21] Additionally, introducing an aryl fused indole into the polymethine structure has led to the development of highly π-conjugated dyes, such as FD-1080, which exhibit efficient SWIR absorption/emission.[22] Donor–acceptor–donor dyads with bulky donors or strong acceptors, exemplified by CH-1055[23] and its variants,[24,25] have also been explored. However, these modifications often significantly impact biocompatibility and aqueous solubility, necessitating the identification of novel cores that exhibit the properties required for bioimaging applications.

The xanthene core (rhodamine, Rdn) has garnered significant attention over the past decade due to its favourable properties for bioimaging. By substituting the bridging C10-oxygen in xanthene with various elements or modifying the amine donors, absorption (λ_{abs}) and emission (λ_{Em}) have been redshifted, though predominantly remain below 800 nm.[26] Recently, the introduction of an electron-withdrawing C=O group has shifted absorption to 860 nm and emission above 1000 nm by affecting the orbital energy levels.[13] The bis-benzannulation (naphthalene embedded) to Rdn with a silicon at the core has been reported, that exhibited λ_{abs} >860 and λ_{Em} > 900 nm.[27]

[a] *Institute of Organic Chemistry, RWTH Aachen University, 52074 Aachen, Germany*
[b] *Kaer Labs, 44300 Nantes, France*
[c] *Department of Functional Imaging in Surgical Oncology, National Center for Tumor Diseases (NCT/UCC), Dresden, Germany*
[d] *German Cancer Research Center (DKFZ), Heidelberg, Germany*
[e] *Medizinische Fakultät and University Hospital Carl Gustav Carus, Technische Universität Dresden, Dresden, Germany*
[f] *Helmholtz Zentrum Dresden-Rossendorf (HZDR), Dresden, Germany*
[g] *Helmholtz Pioneer Campus, Helmholtz Zentrum München, Neuherberg, Germany*
[h] *Biological and Environmental Science Division, King Abdullah University of Science and Technology (KAUST), Thuwal 23955-6900, Saudi Arabia*
[i] *KAUST Catalysis Centre (KCC), King Abdullah University of Science and Technology (KAUST), Thuwal 23955-6900, Saudi Arabia*
[j] *Institute for Experimental Molecular Imaging (ExMI), University Clinic Aachen, 52074 Aachen, Germany. E-mail: sbanala@ukaachen.de srinivas.banala@oc.rwth-aachen.de*

† Electronic supplementary information (ESI) available: Experimental procedure and the characterisation data of all the compounds. See DOI: https://doi.org/10.1039/d4cc05248j

Another notable development is the complete removal of the oxygen atom in rhodamine, resulting in altered optical properties (*e.g.*, a hybrid of fluorene-rhodamine core, FluRdn core).[12]

We have also been interested in preparing novel chromophores suitable for bioimaging applications.[28] In our efforts to develop SWIR emitting cores, we aimed to influence the electronic properties of the 3,6-dimethylamino fluorenone core through its C9-position to induce changes in optical properties. Here we report the synthesis of a new small molecule dye with a molecular weight of 381 Da, which exhibited absorption and emission maxima at 1012 nm and 1100 nm, respectively. Using a SWIR InGaAs camera-based imaging system and longpass filters, we detected fluorescence above 1300 and 1400 nm, confirming that the favourable design of extending π-conjugation can be used to redshift the emission.

To identify substituents that influence the optical properties, we adopted a building block approach, enabling C9 modifications at the final stage on the central building block, 3,6-dimethylamino fluorenone (**5**, Scheme 1). The core **5** was synthesized through a multi-step reaction sequence (see ESI†). To introduce different groups at the C9-position, we explored substitution with aryl–metal reagents prepared *via* metal–halogen exchange reactions using either BuLi or Mg (Grignard). Alongside 2-methylphenyl (**6**) as a reference, we utilized an electron-rich *p*-methoxyphenyl (**7**), its extended conjugation version with an alkyne (**9**), and a lactone forming 2-carboxylic phenyl (**8**) as well as an electron-poor 3,5-bis(trifluoromethyl)phenyl. The pre-prepared reagents (**6–8**) were added under low-temperature conditions to **5**. After 1 h of stirring, the reactions mixture was quenched, yielding the corresponding fluoren-9-ol products with over 85% yield. These were conveniently isolated and thoroughly characterised. Subsequent dehydration was carried out under acidic conditions at room temperature to obtain the corresponding dyes, **1–3**, which were recrystallized in CH_2Cl_2/Et_2O. Product **4** was formed spontaneously *in situ* from the fluoren-9-ol intermediate. To mimic rhodamine B, diethylamino fluorenone **5b** was also employed in the Grignard reaction with *o*-tolyl (**6**) and *o*-methoxyphenyl (**11**) substituents, and subsequent dehydration gave **1b** and **10**. The obtained compounds were characterised by 1D, 2D-NMR and mass spectrometry, confirming their identity.

Subsequently, the optical properties of dyes **1–3** and **10** were investigated. These dyes were dissolved in DMSO, and their absorption was measured at concentrations ranging from 50 μM to 5 μM (see ESI,† Fig. S4–S6). Furthermore, the pH dependency of absorption fluorescence emission for **1b** and **10** was also measured (Fig. S7–S10, ESI†), to observe quenching in basic medium. Compound **4** was found to be stable in its lactone form, which hampered its optical characterisation.

The FluRdn dyes **1–3** and **10** exhibited absorption, emission in the SWIR region, and maxima above 940 nm, and 1000 nm, respectively (see Fig. 1 and Table 1), with rather broad absorption peaks and low molar absorption coefficient (ε) ranging from 4710 M^{-1} cm^{-1} (for **3**) to 12 820 M^{-1} cm^{-1} (for **2**). An electron donating *p*-methoxyphenyl substituent at the C9-position (in **2**) showed slightly stronger absorption and emission than **1**, but with a blue shifted maximum. Introduction of an alkyne in between the *p*-methoxyphenyl and fluorene core (in compound **3**) induced a redshift of 76 nm but resulted in a weaker absorbance and emission compared to **2**. The fluorescence quantum yield (ϕ_{fl}) of FluRdn **1b**, **10** was determined as 0.005% and 0.004% (in DMSO), respectively, using IR-1060 (ϕ_{fl} = 0.32%) and IR-26 (ϕ_{fl} = 0.048%) as references (see ESI,† Fig. S11 and S12) by the relative method.[29] Despite their low quantum yield, they are comparable to NIR-II emitting organic dyes, which typically exhibit low ϕ_{fl} values ranging from 0.001–1%.[30] For comparison, a broadly explored D–A–D dyad for SWIR imaging with a benzo-bisthiadiazole core,[31,32] with two bulky triarylamine donors, *e.g.*, CH1055 exhibits absorption/emission, λ_{abs} = 750 nm/λ_{Em} = 1055 nm of with a ϕ_{fl} 0.098% (in PBS).[23] Thus, the FluRdn could be suitable as an alternative to D–A–D dyes in studying SWIR imaging applications. In comparison to polymethine dyes, which have a much

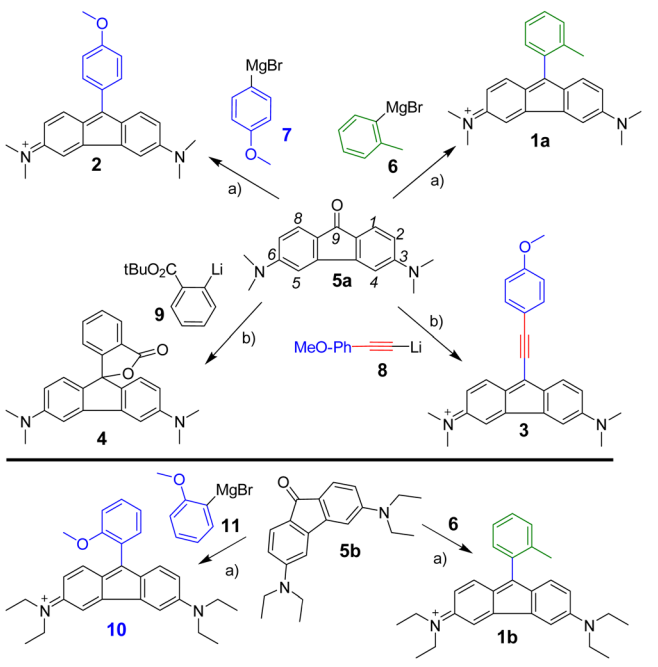

Scheme 1 Synthesis of SWIR dyes in a building block approach from 3,6-dimethylamino fluorenone (**5**). (a) (i) In THF, < −20 °C, warmed to 0 °C; (ii) TFA in $CDCl_3$ at r.t. to 40 °C. (b) In THF, < −78 °C, (ii) TFA in $CDCl_3$ at r.t. to 40 °C.

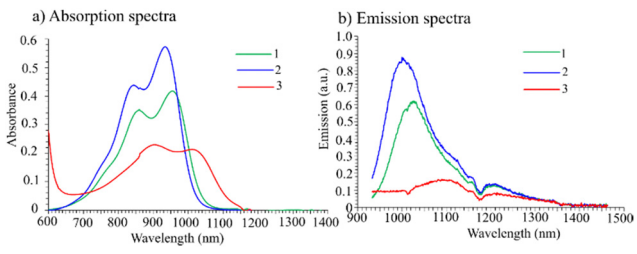

Fig. 1 (a) Absorption spectra of **1–3** in DMSO (50 μM); (b) emission spectra from 933 to 1463 nm in DMSO of 10 μM (the dip at 1160 nm was due to an absorption peak of DMSO). DMSO also showed Raman peaks, and the displayed emission spectra have been corrected for this.

Table 1 Experimentally measured optical properties

Compd.	λ_{abs} (2nd band max, nm)	λ_{Em} max (nm)	Stokes shift (nm)	ε (M^{-1} cm^{-1})	Quantum yield (ϕ_{fl})
1a	954	1026	72	9156	na
1b	965	1035	70	7802	0.005%
2	934	1004	70	12 820	na
10	974	1038	62	8425	0.004%
3	1012	1100	88	4710	na

higher cross-section and consequently higher brightness, these new dyes are much smaller and could potentially be the core for newly developed cell penetrating SWIR probes comparable to other probes with the rhodamine scaffold.

To characterise the imaging performance of the FluRdn core, we explored SWIR imaging using the Kaer Imaging System (KIS from Kaer Labs, Nantes). The KIS system uses a 980 nm laser (also equipped with an 808 nm laser) for excitation and an InGaAs camera for collecting the emitted photons up to 1700 nm, with different longpass (LP) filters ranging from 1050 to 1500 nm to filter the emissions in those wavelengths. The system uses a method to subtract the background (without laser excitation) from the observed SWIR fluorescence and overlays it with a white LED reflectance image for visualization in real-time (Fig. S1 and S3, ESI†). Upon using an LP filter of 1050 nm (collecting emitted photons between 1050–1700 nm), dyes **1** and **2** exhibited a signal-to-background-ratio (SBR) of >16 in SWIR imaging (see Fig. S2, ESI†). Dye **1** produced a slightly higher SBR, while dye **2** exhibits a little lower SBR, probably due to the 980 nm laser excitation where **2** has a lower absorbance (ε), resulting in fewer emitted photons and yielding a lower SBR. To our surprise, dye **3** performed well in SBR, despite its weak absorption and emission.

Then, we performed SWIR camera-based fluorescent imaging of the solutions with three additional LP filters (1200, 1300 and 1400 nm) using 980 nm laser excitation (Fig. 2). Changing the LP filter to capture longer wavelength photons markedly increased the imaging performance. Although the total number of collected photons (signal density) decreased with increasing LP filter cut-off, the SBR increased slightly for the 1200 nm LP while a drop was observed for 1300 nm and 1400 nm LP. To capture emission >1400 nm, the exposure time had to be adjusted to 2 s. This highlights the usefulness of the FluRdn core for detection in >1300 nm imaging.

To understand the observed optical data in relation to the electronic nature of the substituents, time-dependent density functional theory (TD-DFT) calculations were performed using the PBE0[33] functional and def2-TZVPP[34] basis sets on the optimized geometries at the wB97xD/def2-TZVP level of theory.[35] The Gaussian 16 software[36] was used for geometry optimizations and TD-DFT calculations. The solvent effects using the program implicitly embedded dielectric constant (DMSO: 46.826, water: 78.3553) were evaluated, by a self-consistent reaction field (SCRF) approach using the SMD continuum solvation model[37] for geometry optimization and TD-DFT calculations.[38] The calculated λ_{max} (**1**: 745 nm, **2**: 731 nm, **3**: 793 nm) was underestimated by up to 200 nm in both the solvents, compared to the experimental data (see Fig. S13, ESI†), including the Rdn (calcd λ_{max}: 467 nm) dye. The TD-DFT predicted oscillator strengths and molar absorption in the SWIR region are similar to all the FluRdn dyes (Fig. S13 and Table S1, in ESI†). However, the influence of C9-substituents on the orbital levels is clearly observed (Fig. 3).

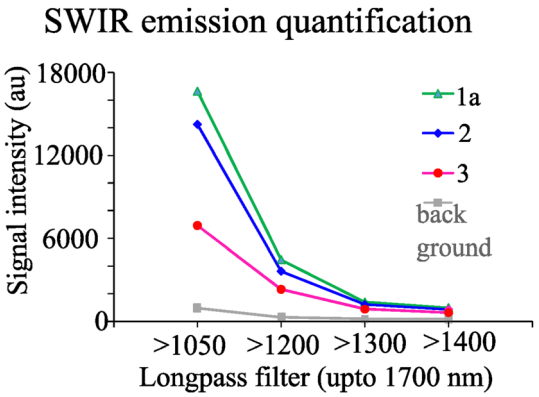

Fig. 2 Quantification of the SWIR fluorescence signal with four LP filters (collected emission was from LP cut-off to 1700 nm, exposure time. 1 s for up to 1300 and LP 1400 nm: 2 s) of the three dyes.

In the geometries of **1–3**, the highest occupied molecular orbitals (HOMOs) were mainly localized on the fluorene core. The observed negligible difference in HOMO energy levels ($\Delta E_{HOMO} \leq \pm 0.01$ eV) confirms this conclusion. Among the lowest unoccupied molecular orbitals (LUMOs), it was mainly localized at the fluorene in **1** and **2**, but not in **3**. A contribution of ethynyl orbitals on the LUMO (but not the substituent *p*-methoxy phenyl effect) could be seen in **3**, indicating that the C9-conjugation influences the observed optical properties. The effect of the ethynyl group in **3** on energy levels could also be seen qualitatively in the narrowing energy gap (E_{gap} = 4.9 *vs.* 5.15 eV for **2**), that was reflected in a redshift of 78 nm. This confirms that the

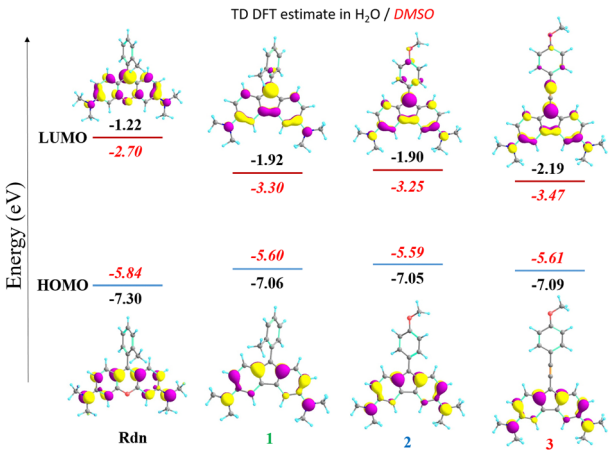

Fig. 3 The frontier molecular orbitals (HOMO/LUMO; isosurface = 0.05 a.u.) with energies (in eV, in H_2O/DMSO) associated to the λ_{max} are presented. The effect of the C-9 substituent on the HOMO/LUMO energy levels of the three FluRdn dyes (**1–3**), along with rhodamine (Rdn), is analysed to understand its influence.[38]

C9-substituent could be used for further fine-tuning of the optical properties. This is in contrast to Rdn, in which both the HOMO and LUMO are localized in the xanthene core.

In conclusion, we have demonstrated the fine-tuning of the optical properties of FluRdn, its potential for SWIR imaging applications, and the use of TDDFT calculations to explore the electronic effects on these properties. This study highlights the potential of substituting conjugatable groups at the C9-position to achieve red-shifted emissions. As SWIR imaging becomes increasingly important in real-time visualization of blood vessels, lymphatics, angiography, and tumour resection, the limitations of current probes underscore the need for novel SWIR agents with less non-specific binding, efficient extra vascularization and fast clearance. The FluRdn core presented here shows significant promise due to its small size and hydrophilicity, making it suitable for further development. Furthermore, the introduction of other substituents at peripheral positions, and fusing of electron-rich amine donors, embedding julolidine into the FluRdn core, creates interesting scaffolds, which could also be fine-tuned with the methods discussed here in refining optical properties, which is currently ongoing in our laboratories.

S. B. gratefully acknowledges the financial support from the Central Innovation for SMEs (ZIM) of the German Federal Ministry for Economic Affairs and Climate Action (BMWK). Help from Amir Gizatullin (KCC, KAUST) is gratefully acknowledged for providing **5b**. O. T. B. acknowledges funding from Helmholtz Zentrum München core funding, National Center for Tumor Diseases (NCT) core funding, Deutsche Forschungsgemeinschaft (DFG) Emmy Noether program no. BR 5355/2-1, German Federal Ministry of Education and Research (BMBF) project BetterView, Helmholtz Imaging Project grant ZT-I-PF-4-038, Chan Zuckerberg Initiative (CZI) Deep Tissue Imaging grants DTI-0000000248 and DTI2-0000000206, and Deutsche Forschungsgemeinschaft (DFG) SFB1123-B10.

Data availability

The data supporting this article have been included as part of the ESI.†

Conflicts of interest

P. A. D. is a co-founder of and has shares in the company Kaer Labs.

References

1 M. Bai, *In Vivo Fluorescence Imaging: Methods and Protocols*, Springer, New York, 2016.
2 T. Sun, H. Zhao, L. Hu, X. Shao, Z. Lu, Y. Wang, P. Ling, Y. Li, K. Zeng and Q. Chen, *Acta Pharm. Sin. B*, 2024, **14**, 2428–2446.
3 C. Ash, M. Dubec, K. Donne and T. Bashford, *Lasers Med. Sci.*, 2017, **32**, 1909–1918.
4 Z. Zhang, Y. Du, X. Shi, K. Wang, Q. Qu, Q. Liang, X. Ma, K. He, C. Chi, J. Tang, B. Liu, J. Ji, J. Wang, J. Dong, Z. Hu and J. Tian, *Nat. Rev. Clin. Oncol.*, 2024, **21**, 449–467.
5 F. Wang, Y. Zhong, O. Bruns, Y. Liang and H. Dai, *Nat. Photonics*, 2024, **18**, 535–547.
6 C. Li, G. Chen, Y. Zhang, F. Wu and Q. Wang, *J. Am. Chem. Soc.*, 2020, **142**, 14789–14804.
7 S. Diao, J. L. Blackburn, G. Hong, A. L. Antaris, J. Chang, J. Z. Wu, B. Zhang, K. Cheng, C. J. Kuo and H. Dai, *Angew. Chem., Int. Ed.*, 2015, **54**, 14758–14762.
8 L. Tong, J. Cao, K. Wang, J. Song and J. Mu, *Adv. Opt. Mater.*, 2024, **12**, 2301767.
9 O. T. Bruns, T. S. Bischof, D. K. Harris, D. Franke, Y. Shi, L. Riedemann, A. Bartelt, F. B. Jaworski, J. A. Carr, C. J. Rowlands, M. W. B. Wilson, O. Chen, H. Wei, G. W. Hwang, D. M. Montana, I. Coropceanu, O. B. Achorn, J. Kloepper, J. Heeren, P. T. C. So, D. Fukumura, K. F. Jensen, R. K. Jain and M. G. Bawendi, *Nat. Biomed. Eng.*, 2017, **1**, 0056.
10 S. Diao, J. L. Blackburn, G. Hong, A. L. Antaris, J. Chang, J. Z. Wu, B. Zhang, K. Cheng, C. J. Kuo and H. Dai, *Angew. Chem., Int. Ed.*, 2015, **54**, 14758–14762.
11 Q. Miao and K. Pu, *Adv. Mater.*, 2018, **30**, 1801778.
12 M. Grzybowski, O. Morawski, K. Nowak and P. Garbacz, *Chem. Commun.*, 2022, **58**, 5455–5458.
13 H. C. Daly, S. S. Matikonda, H. C. Steffens, B. Ruehle, U. Resch-Genger, J. Ivanic and M. J. Schnermann, *Photochem. Photobiol.*, 2022, **98**, 325–333.
14 V. G. Bandi, M. P. Luciano, M. Saccomano, N. L. Patel, T. S. Bischof, J. G. P. Lingg, P. T. Tsrunchev, M. N. Nix, B. Ruehle, C. Sanders, L. Riffle, C. M. Robinson, S. Difilippantonio, J. D. Kalen, U. Resch-Genger, J. Ivanic, O. T. Bruns and M. J. Schnermann, *Nat. Methods*, 2022, **19**, 353–358.
15 E. D. Cosco, A. L. Spearman, S. Ramakrishnan, J. G. P. Lingg, M. Saccomano, M. Pengshung, B. A. Arús, K. C. Y. Wong, S. Glasl, V. Ntziachristos, M. Warmer, R. R. McLaughlin, O. T. Bruns and E. M. Sletten, *Nat. Chem.*, 2020, **12**, 1123–1130.
16 J. A. Carr, D. Franke, J. R. Caram, C. F. Perkinson, M. Saif, V. Askoxylakis, M. Datta, D. Fukumura, R. K. Jain, M. G. Bawendi and O. T. Bruns, *Proc. Natl. Acad. Sci. U. S. A.*, 2018, **115**, 4465–4470.
17 S. Zhu, B. C. Yung, S. Chandra, G. Niu, A. L. Antaris and X. Chen, *Theranostics*, 2018, **8**, 4141–4151.
18 S. Zhu, Z. Hu, R. Tian, B. C. Yung, Q. Yang, S. Zhao, D. O. Kiesewetter, G. Niu, H. Sun, A. L. Antaris and X. Chen, *Adv. Mater.*, 2018, **30**, 1802546.
19 Q. Liu, Y. Zhong, Y. Su, L. Zhao and J. Peng, *Nano Lett.*, 2021, **21**, 4606–4614.
20 E. D. Cosco, J. R. Caram, O. T. Bruns, D. Franke, R. A. Day, E. P. Farr, M. G. Bawendi and E. M. Sletten, *Angew. Chem., Int. Ed.*, 2017, **56**, 13126–13129.
21 B. Ding, Y. Xiao, H. Zhou, X. Zhang, C. Qu, F. Xu, Z. Deng, Z. Cheng and X. Hong, *J. Med. Chem.*, 2019, **62**, 2049–2059.
22 B. Li, L. Lu, M. Zhao, Z. Lei and F. Zhang, *Angew. Chem., Int. Ed.*, 2018, **57**, 7483–7487.
23 A. L. Antaris, H. Chen, K. Cheng, Y. Sun, G. Hong, C. Qu, S. Diao, Z. Deng, X. Hu, B. Zhang, X. Zhang, O. K. Yaghi, Z. R. Alamparambil, X. Hong, Z. Cheng and H. Dai, *Nat. Mater.*, 2016, **15**, 235–242.
24 H. Ma, C. Liu, Z. Hu, P. Yu, X. Zhu, R. Ma, Z. Sun, C.-H. Zhang, H. Sun, S. Zhu and Y. Liang, *Chem. Mater.*, 2020, **32**, 2061–2069.
25 Q. Yang, H. Ma, Y. Liang and H. Dai, *Acc. Mater. Res.*, 2021, **2**, 170–183.
26 L. D. Lavis, *Ann. Rev. Biochem.*, 2017, **86**, 825–843.
27 J. Li, Y. Dong, R. Wei, G. Jiang, C. Yao, M. Lv, Y. Wu, S. H. Gardner, F. Zhang, M. Y. Lucero, J. Huang, H. Chen, G. Ge, J. Chan, J. Chen, H. Sun, X. Luo, X. Qian and Y. Yang, *J. Am. Chem. Soc.*, 2022, **144**, 14351–14362.
28 J. M. Merkes, T. Lammers, R. Kancherla, M. Rueping, F. Kiessling and S. Banala, *Adv. Opt. Mater.*, 2020, **8**, 1902115.
29 H. Piwoński, S. Nozue and S. Habuchi, *ACS Nanosci. Au*, 2022, **2**, 253–283.
30 Z. Lei and F. Zhang, *Angew. Chem., Int. Ed.*, 2021, **60**, 16294–16308.
31 G. Qian, B. Dai, M. Luo, D. Yu, J. Zhan, Z. Zhang, D. Ma and Z. Y. Wang, *Chem. Mater.*, 2008, **20**, 6208–6216.
32 L. Wang, N. Li, W. Wang, A. Mei, J. Shao, W. Wang and X. Dong, *ACS Nano*, 2024, **18**, 4683–4703.
33 C. Adamo and V. Barone, *J. Chem. Phys.*, 1999, **110**, 6158–6170.
34 F. Weigend and R. Ahlrichs, *Phys. Chem. Chem. Phys.*, 2005, **7**, 3297–3305.
35 J.-D. Chai and M. Head-Gordon, *Phys. Chem. Chem. Phys.*, 2008, **10**, 6615–6620.
36 M. J. Frisch, *et al.*, *Gaussian 16 rev C.02*, Gaussian Inc., 2019.
37 A. V. Marenich, C. J. Cramer and D. G. Truhlar, *J. Phys. Chem. B*, 2009, **113**, 6378–6396.
38 D. Jacquemin, E. A. Perpète, G. E. Scuseria, I. Ciofini and C. Adamo, *J. Chem. Theory Comput.*, 2008, **4**, 123–135.